VOF modelling of gas–liquid flow in PEM water electrolysis cell micro-channels

Lafmejani, Saeed Sadeghi; Olesen, Anders Christian; Kær, Søren Knudsen

Published in:
International Journal of Hydrogen Energy

DOI (link to publication from Publisher):
10.1016/j.ijhydene.2017.05.079

Publication date:
2017

Document Version
Accepted author manuscript, peer reviewed version

VOF modelling of gas—liquid flow in PEM water electrolysis cell micro-channels

Saeed Sadeghi Lafmejani, Anders Christian Olesen, Søren Knudsen Kær

Department of Energy Technology, Aalborg University, 9220 Aalborg East, Denmark

Abstract

In this study, the gas—liquid flow through an interdigitated anode flow field of a PEM water electrolysis cell (PEMEC) is analysed using a three-dimensional, transient, computational fluid dynamics (CFD) model. To account for two-phase flow, the volume of fluid (VOF) method in ANSYS Fluent 17.2 is used. The modelled geometry consists of the anode channels and the anode transport layer (ATL). To reduce the complexity of the phenomena governing PEMEC operation, the dependence upon electro-chemistry is disregarded. Instead, a fixed source of the gas is applied at the interface between the ATL and the catalyst layer. An important phenomenon that the model is able to capture is the gas—liquid contact angle on both the channel wall and ATL-channel interface. Particularly, the latter interface is crucial in capturing bubble entrainment into the channel. To validate the numerical simulation, photos taken of the gas—liquid flow in a transparent micro-channel, are qualitative compared against the simulation results. The experimental observations confirm the models prediction of long Taylor bubbles with small bubbles in between. From the simulation results, further intriguing details of the flow are revealed. From the bottom to the top of the outgoing channel, the film thickness gradually increases from zero to 200 m. This increase in the film thickness is due to the particular superficial velocity field that develops in an interdigitated flow. Here both the superficial velocities change along the length of the channel. The model is capable of revealing effect of different bubble shapes/lengths in the outgoing channel. Shape and the sequence of the bubbles affect the water flow distribution in the ATL. The model presented in this work is the first step in the development of a comprehensive CFD model that comprises multiphase flow in porous media and micro-channel, electro-chemistry in catalyst layers, ion transport in membrane, hydrogen evolution, etc. The model can aid in the study of gas—liquid flow and its impact on the performance of a PEMEC.

Keywords:
PEMEC, Water electrolysis, Single-fluid VOF, CFD, gas—liquid flow, Taylor flow

1. Introduction

It is highly agreed that the emission of greenhouse gases (GHG) is the greatest cause of global warming. A large fraction of the emitted GHG originate from the use of fossil fuels in energy production and transportation [1]. Denmark has started using different methods for the green transition. An energy agreement was signed by Danish government in 2012 with the target of supplying at least 50% of the electricity consumption using wind power by 2020. Moreover, the target claims that 35% of the total consumption of energy should be supplied from renewable energy sources. To achieve these targets, a full reorganisation of the energy matrix with renewable sources is required [2]. Such a transition needs a high degree of energy availability and storage capacity of secondary fuels produced from electricity. Here, electrolysers play a vital role as a means of converting and storing energy. By converting water and electricity into hydrogen, an efficient energy carrier is produced. As a chemical compound, hydrogen is furthermore useful in various applications; from production of chemicals to fuel cell based vehicles [3, 4, 5].

Water electrolysis will play a key role in the future renewable energy system to facilitate storage of intermittent renewable energy from wind and sun. The key challenge facing the hydrogen based energy production is sustainable production of hydrogen, without dependence on fossil fuels, in large quantities at lower costs than existing technologies [6].

Unlike Alkaline water electrolysers, proton exchange membrane electrolysis cells (PEMEC), offer significantly higher current densities, and in turn a more compact design. Even with the expensive noble metals as an electrocatalyst that the technology uses at the current time, its capabilities such as large load range (10-200%), rapid dynamic response and high operating pressure are supposed to overcome its drawbacks [7]. One of the methods for reducing price of PEMECs is to increase production per cell active area.

Han et. al. [8] one-dimensionally modelled gas—liquid flow inside ATL. They captured the limiting value of current density by increasing voltage. They depicted that the ATL contact angle, porosity and thickness has a great impact on ATL. They concluded that high ATL porosity and low surface contact angle improves PEMEC performance

at high current densities. Yigit et. al. [9] have done dynamic simulation of a PEMEC system using Simulink in MATLAB. Their study showed stack has the highest loss than other components like water pump, cooling fan and etc, especially at high current density. Tijani et. al. [10] studied effect of different temperatures, pressures and membrane thicknesses on the performance of a PEM electrolyser. They found that by increasing current density, Faraday efficiency increases but by decrease in membrane thickness, Faraday efficiency decreases.

Regular PEM water electrolysers are commonly operated at a current density of about $1(A/cm^2)$. One means of increasing the hydrogen to cost ratio of the technology, is to increase the operating current density. This statement holds true, since the major cost of the system is the fixed cost associated with building the electrolyser. Thus, by simply increasing the production yield, the hydrogen to cost ratio has to decrease. Therefore, heat and mass transfer management in the anode liquid/gas diffusion layer (ATL) at high current densities becomes essential.

These conditions may cause maldistribution of heat and water. By improving the cell performance for high current density condition, the technology will be matured for hydrogen production in large scales with high a efficiency. This necessitates that more understanding of the gas—liquid flow in both the ATL and the micro-channel from both numerical and experimental methods are crucial. Therefore, knowledge of the flow pattern forming under a given inlet and operational condition is essential for predicting the behaviour of gas—liquid flow in micro-channels.

Six major flow regimes can be distinguished in micro-channels [11]: bubbly and Taylor flows that are dominated by surface tension, the churn and Taylor-annular flows that are transitional, and the dispersed and annular flows that are inertia dominated. According to the literature, channel size, phase superficial velocities, liquid phase surface tension, wall wettability and inlet conditions affect flow pattern. Meanwhile, the channel cross sectional geometry, liquid viscosity and flow orientation respecting the gravity has a lower degree of importance. The flow regime map is highly dependent on the inlets used in the various studies as well as different wall properties, such as wettability, contamination and roughness. Figure .1 shows five different flow regimes encounters in micro-channels [11].

Figure. 4 shows the gas—liquid (i.e. water-nitrogen) flow regime map of a vertical triangular channel with a hydraulic diameter of 0.55 mm. The flow map is used for selecting an appropriate operating condition for this study. The blue continuous line shows a roughly estimated gas and liquid superficial velocity from bottom to top of the channel. The estimation assumes a uniform flow of gas and liquid from ATL to the channel. The channel is vertical with a hydraulic diameter close to that of this study, i.e. 0.66 mm. As Fig. 10 shows, most of the gas—liquid flow in the PEMEC micro-channels should be Taylor. Therefore, from hereon, a literature review of the methods of

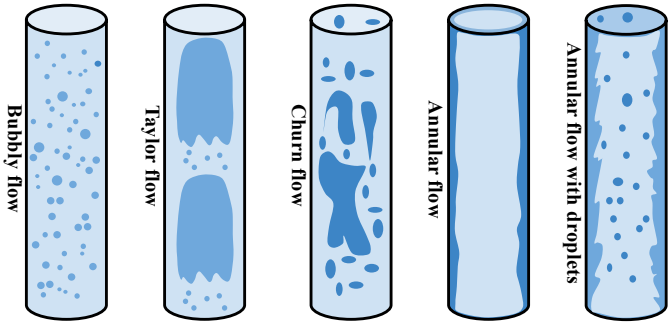

Figure 1: gas—liquid flow regimes in micro-channels.

modelling Taylor flow is presented.

Shao et al. [11] depicted in their review paper, that the flow regimes map slightly differs between vertical and horizontal channels. There is a larger interest for gas—liquid flow to stay in Taylor flow regime in a horizontal channel than a vertical one. Furthermore, it is highly dependent on the channel diameter. The area in the flow regime map for Taylor flow in a channel increases by reducing the channel diameter and the flow gets into the bubbly flow regime at higher liquid velocities in a smaller channel than a large one. Also the flow gets into dispersed flow regime at higher velocities for both gas and liquid. It is also mentioned that the shape of the channel and contact angle has a very small impact on the flow regime map. Liquid surface tension has a high impact on the flow regime, as it shows a higher interest to the Taylor flow at higher liquid surface tensions. They also reported that a $U_{LS} - U_{GS}$ as coordinates, better represents the transition between flow regime maps than $ReWe_{LS} - ReWe_{GS}$.

Even though it is possible to map the borders between the different flow regimes of a specific gas—liquid flow and channel configuration, it is very difficult to create a generalised flow pattern map that is valid for all fluid and wall properties as well as channel dimensions. CFD modelling can help analysing the effects of different parameters on flow patterns in PEM electrolysers. It is a useful tool for visualising and understanding the physics at play. Analysing cell heat and mass transport gives considerable ability in understanding the phenomenon and improving the cell performance for high current densities. Moreover, it helps in identifying critical issues that take long time and are costly to find in experimental investigations.

Unlike modelling of the PEM fuel cell, which dates back to the early 1990s, the modelling of PEMEC is still in its early stages of development, with the earliest models reported in 2002 [2]. Modelling of PEM fuel cell is closely related in many aspects and it is already well established with several good review papers available [12, 13, 14, 15, 16, 17, 18]. Bensmann et al. [19] in their review paper mentioned that only a few contributions thoroughly consider gas—liquid flow in the ATL. Even though the PEMEC flow fields is a boundary layer for PEMEC, that is important from fluid dynamics and heat transfer view-

points, majority of publications present a simple model for it. Understanding the two-phase flow influence on PEMEC performance and the cell pressure resistance especially at high current densities and large cells needs a detailed [20, 21]. Bensmann recommended the consideration of two-phase model from other applications like geology [19].

The latest numerical study of a PEMEC was done by Olesen et al. 2016 [7]. They investigated the use of a circular-planar, inter-digitated flow field for the anode of a high pressure PEMEC in a numerical study. They developed both single phase and two phase flow models to study the effect of geometry and the dispersed gas bubbles. The results showed that the cell performance is highly dependent on the bubble size.

As Fig. 4 shows, most of the gas—liquid flow in the PEMEC micro-channels should be Taylor. Therefore, from hereon, a literature review of the methods of modelling Taylor flow is presented. There are many researchers worked on simulating gas—liquid Taylor flow in micro-channels. De Schepper et al. [22] modelled gas—liquid flow in horizontal channels using VOF model. Gupta et al. [23], CFD modelled Taylor flow in micro-channel using VOF method. They reviewed the existing literature and made some recommendation on the mesh sizes to capture wall liquid film. Gupta et al. [24] CFD modelled flow and heat transfer of gas—liquid Taylor flow in micro-channel using VOF and level-set techniques by two different codes: ANSYS Fluent and TransAT. Du et al. [25] investigated gas—liquid two-phase flow in mini-channels with liquid side introduction. Asadolahi et al. [**?**] used VOF method to model hydrodynamics and heat transfer in Taylor flow by implementing two different approaches of moving mesh and moving frame. Asadolahi et al. [**?**] CFD modelled gas—liquid flow in a 2 mm diameter micro-channel with Reynolds number in the range of 22-1189 using VOF model of ANSYS Fluent. They used 2D, periodic flow in a moving reference frame (MRF) with the bubble and were able to capture the bubble shape, liquid film thickness and bubble velocity. Gupta et al. [**?**] both numerically and experimentally analysed long liquid droplets in another liquid phase in a micro-channel of 1.06 mm diameter. Here also they used VOF method to model Taylor flow. Dai et al. [**?**] has also done a similar work using VOF method. All these researchers used VOF method for modelling gas—liquid Taylor flow in micro-channels.

The aim of this study is to initially model gas—liquid flow in PEMEC inter-digitated anode flow field micro-channels using a microscopic, three-dimensional VOF model. The model will be a base for further and detailed modelling of electro-chemistry and gas—liquid flow in PEMECs. A well developed model could be used for better understanding the phenomena happening in PEMEC, finding maldistribution areas, optimising the flow fields and probably recommendations for higher performance.

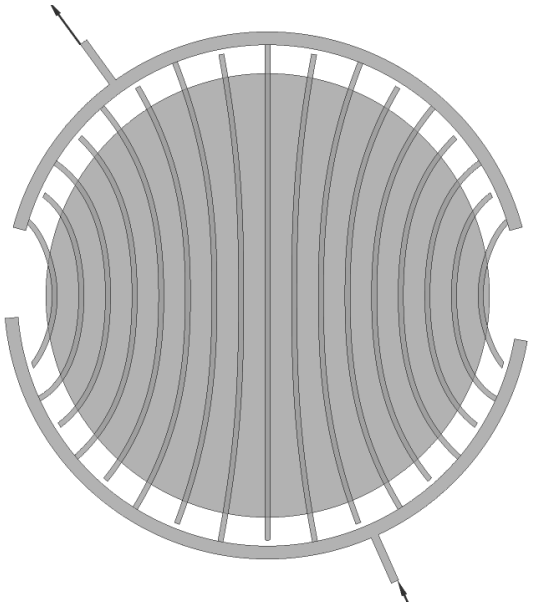

Figure 2: The full cell.

2. Methodology

2.1. Geometry

Figure. 2 shows the circular inter-digitated PEMEC channels. It has 8 incoming and 9 outgoing channels which transport liquid and gas to and from the ATL (Ti-felt). Water flows from the incoming channels into the ATL, where it by advection assists in removing the accumulated oxygen. From within the ATL, the developed gas—liquid mixture then flows into the outgoing channel. Due to high operating pressure of the cathode, the channels are designed very thin in comparison to the land width. The curved channels helps achieve a more uniform distribution of water and gas throughout the ATL.

Simulating the whole circular geometry demands a high number of cells (i.e. more than 17 million). Solving such a simulation case would require several months of computational time with a 16 cores workstation. Spending that amount of time is unfeasible for parametric studies. To reduce simulation time, only a part of the geometry has been selected. For the sake of simplicity, the three straight channels in the middle of the cell are selected. The geometry is shown in Fig. 3. There is a 4mm spacing between them as land area. Channels have a width of 1mm, length of 94 mm and the depth of 0.5 mm. The transparent setup has an active area of 11 by 94 mm. The active area is a porous media and is made of Titanium felt (Ti-felt).

2.2. Porous medium

The membrane electrode assembly (MEA) typically consist of a thick membrane like Nafion 117 that is coated with a layer of catalyst on each side. On top of this catalyst coated membrane (CCM), porous structures are added to both sides for an optimal reactant and product distribution. For the cathode and anode, respectively, a carbon

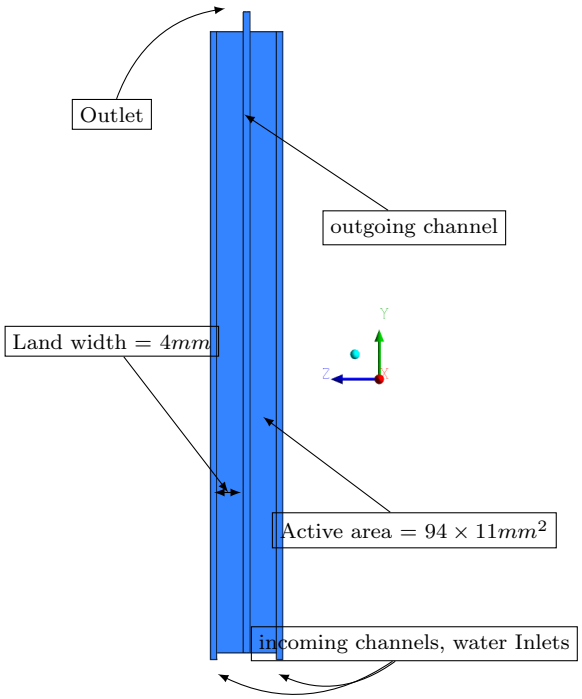

Figure 3: A slice of the 3D geometry.

and titanium based material are used. Current is transferred to the MEA from the bipolar plates through a hydrophilic porous medium that in this study is just titanium (Ti). There are three structures for the titanium: screen mesh, sintered powder and unwoven random fibres (felt). The porous media plays a great role in water/oxygen transport to and from the catalyst layer. In this study, the ATL (made of Ti-felt) is a fibrous structure that has a thickness of 350 µm with fibre diameter of 20 µm. Its weight is 300 $\frac{g}{cm^2}$ with the volume porosity of 81%. Porosity of the Ti-felt depends on compression pressure and initial porosity without compression as follows [**?**]:

$$\epsilon = 1 - \frac{1}{1-s}(1-\epsilon_0) \tag{1}$$

The initial volume porosity (ϵ_0) is as follows, which the equation was made by fitting a curve on Olesen's experimental data [7]:

$$\epsilon_0 = -3.995 \times 10^{-4} CP + 0.8083 \tag{2}$$

The following equation achieved by fitting a curve on strain-pressure data of Olesen [7]:

$$s = -2.166\times10^{-6}CP^2 + 1.859\times10^{-3}CP + 1.44\times10^{-2} \tag{3}$$

The porous media has a specific permeability which changes by compression pressure as follows:

$$K = (4.439\times10^{-5}CP^2 - 2.2365\times10^{-2}CP + 4.289)\times10^{-11} \tag{4}$$

Table 1: Superficial Reynolds number in channels.

Channel:	incoming	quarters of outgoing			
		1^{st}	2^{nd}	3^{rd}	4^{th}
Reynolds:	864	216	648	1080	1512

The pressure loss due to flow of multiphase flow in the porous media is calculated by Darcy equation:

$$M = \begin{cases} \frac{\mu}{K}u & \Omega \in ATL \\ 0 & \Omega \in Channel \end{cases} \tag{5}$$

Effective viscosity of porous medium on the diffusion term in the momentum equations is introduced by relative viscosity:

$$\mu_e = \mu_r \mu \tag{6}$$

where μ is the fluid viscosity, μ_r is the relative viscosity, and mu_e is the effective viscosity of the porous medium. Breugem correlation is used to calculate relative viscosity:

$$\mu_r = \begin{cases} \frac{1}{2}(\alpha - \frac{3}{7}) & \alpha \geq \frac{3}{7} \\ 0 & \alpha < \frac{3}{7} \end{cases} \tag{7}$$

which α is gas volume fraction.

2.3. Turbulence

In Tab. 1 the superficial Reynolds numbers at specific locations are depicted. The locations are the inlet of the incoming channels as well as at the middle of the first, second, third and fourth quarters of the outgoing. It shows that the water flow is laminar along the channels with the possibility of getting turbulent due to the rapid movement of bubbles at the top of the outgoing channel.

2.4. Assumptions

Numerical modelling of multiphase flow in three dimensional mode, is computationally and timely very expensive. Because of that, a set of assumptions are made in order to reduce the number of solving mathematical equations:

- Since in the compared experimental case, air-water flow is analysed, here Air is selected as the gas phase.
- Bubbles are generated uniformly across the active area surface (means a uniform current density in real condition).
- Existence and flow of bubbles in the incoming channels is neglected (it results in using large cells and saving computation time).
- Laminar flow in the incoming channels and the porous media (results in higher simulation speed).
- Capillary pressure in the porous media is neglected, since single-equation VOF model is used.

- Water phase change is neglected.
- Dissolution of air in water is neglected.
- The process is adiabatic. Fluids are at the same temperature and correspondingly, the energy equation is neglected.

2.5. Mathematical model

The implementation of the VOF method in double precision mode of ANSYS Fluent 17.2 [**?**] is chosen, since it is known to be able to capture the gas—liquid interface that is found in bubbly flows. In this proven method an advection equation is solved for one of the phases, which tracks the interface.

2.5.1. Governing equations

In the VOF method a single-fluid formulation is solved through all the domain, with shared velocity and pressure fields for all the phases. Conservation equations of continuity, momentum, volume fraction and turbulence are solved simultaneously. Together, these equations simulate the fluid flow field and can capture the gas—liquid interface when appropriate closure equations for the surface tension force are introduced.

Continuity:

$$\nabla.\rho\mathbf{V} = 0 \tag{8}$$

Momentum:

$$\frac{\partial(\rho\mathbf{V})}{\partial t}+\nabla.(\rho(\mathbf{V}\otimes\mathbf{V})) = -\nabla p+\mu_e\nabla.(\nabla\mathbf{V}+\nabla\mathbf{V}^T)+\rho\mathbf{g}+\mathbf{F_s}+M \tag{9}$$

Volume fraction:

$$\frac{\partial\alpha}{\partial t} + \mathbf{V}.\nabla\alpha = 0 \tag{10}$$

Turbulence: In order to capture turbulent flow that develops along the outgoing channel, the two-equation, eddy viscosity model, known as Mentors' Shear Stress Transport (SST) model, is used. This method combines advantages of both $k-\epsilon$ and $k-\omega$ methods in free stream and viscous sub-layers correspondingly [**?**].

$$\nabla.(\epsilon\rho\mathbf{V}k - \epsilon(\mu + \frac{\mu_t}{\sigma_k})\nabla k) = P_k - \beta'\rho k\omega + P_{kb} \tag{11}$$

$$\nabla.(\epsilon\rho\mathbf{V}\omega - \epsilon(\mu + \frac{\mu_t}{\sigma_k})\nabla\omega) = \alpha\frac{\omega}{k}P_k - \beta\rho k\omega^2 + P_{\omega b} \tag{12}$$

where $\mathbf{V}$ denotes the velocity vector, p the pressure, ρ the density and μ the dynamic viscosity of the gas—liquid mixture. $\mathbf{F_s}$ is the surface tension force approximated as a body force in the neighbourhood of the interface, and α is the volume fraction of the gas phase. The bulk properties, such as density and viscosity, are determined from the volume-fraction weighted average of the properties of the two fluids.

Intermittency: The model is used to take into account the different flow states as laminar, laminar-turbulent and turbulent. It calculates state of the flow which differs from 0 as indicator of a fully laminar flow, to 1 as fully turbulent flow. The equations can be found in ANSYS Fluent documentation [**?**].

2.5.2. Surface tension model

There are two methods for modelling surface tension in Fluent: Continuum Surface Force (CSF) and Continuum Surface Stress (CSS) [**?**]. The CSF model is selected due to its higher simulation stability. The method adds a source term to the momentum equation to implement surface tension effect. The gas—liquid surface tension is set to $0.072\,(\mathrm{N/m})$. This value corresponds to the air-water surface tension at ambient conditions (i.e. 27 C, 1 atm). The force is calculated by the following equation:

$$\mathbf{F}_S = \sigma\kappa\delta(\mathbf{r}-\mathbf{r}_{int})\mathbf{n} \tag{13}$$

where σ is the coefficient of surface tension, κ is the radius of curvature, $\delta(\mathbf{r})$ is the Dirac delta function and $\mathbf{n}$ denotes the unit normal vector on the interface. The normal $\mathbf{n}$ and curvature κ are defined in terms of the divergence of volume fraction:

$$\mathbf{n} = \frac{\nabla\alpha}{|\nabla\alpha|} \tag{14}$$

and

$$\kappa = \nabla.\mathbf{n} \tag{15}$$

Wall adhesion is activated with a contact angle of 70 degrees. Furthermore, a contact angle of 170 degrees is defined on the "porous-fluid" interface by adding a zero pressure loss porous jump in Fluent to account for the wall effect of Ti-felt and it's high hydrophilic property.

2.5.3. Boundary conditions

Fluid and boundary conditions used in the study are described in detail in Tab. 3. It was decided to choose specific gas and liquid flow rates that would show both bubbly and Taylor flow regimes along the length of the outgoing channel. To ensure this, the two-phase flow map measured in the paper of Zhao et al. [**?**] was selected. They depicted the two-phase flow map of water-nitrogen in a vertical triangular $0.866\,(\mathrm{mm})$ channel. The gas—liquid flow map was chosen since properties of nitrogen and air are close. Furthermore, the hydraulic diameter of their triangular channel is close to the present study. The gas—liquid flow map is shown in Fig. 4. To see both bubbly and Taylor flow regime in the channel, current density of $1(A/cm^2)$ with stoichiometric number of 1000 is selected. The blue continuous line in Fig. 4 depicts the change in gas—liquid superficial velocities along the length of the outgoing channel. The flow map predicts for these conditions that the flow in the first half of the channel should be bubbly, while the second half should be Taylor flow.

Table 2: Calculated wall film thickness

	Film thickness			
	1/8	3/8	5/8	7/8
Thickness (µm)	13	27	37	47

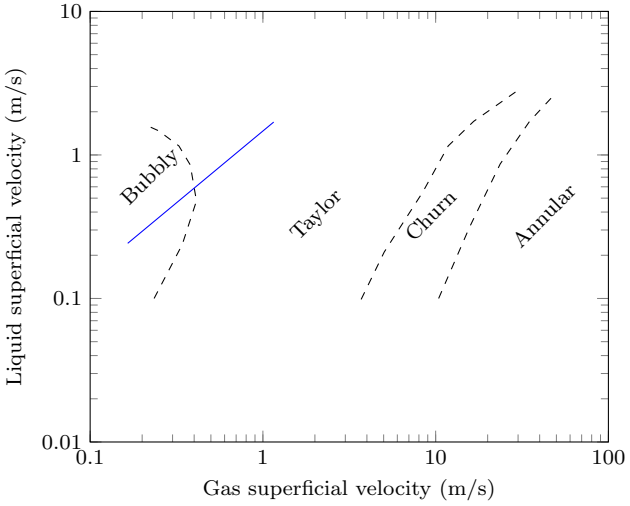

Figure 4: gas—liquid flow regime map in a vertical triangular micro-channel based on liquid and gas superficial velocities [**?**]. The blue line shows the gas—liquid flow regime predicted by the map for the selected gas / liquid inlet condition in this study.

Table 3: Fluid and boundary conditions

Boundary	Value
Surface tension coefficient at Multiphase channel	0.072 [N/m]
Surface tension coefficient at other domain	0 [N/m]
Air density	1.225 (kg/m^3)
Water density	998.2 (kg/m^3)
Air viscosity	1.7894×10^{-5}
Water viscosity	1.003×10^{-3}
Porous formulation	Superficial velocity
Laminar zone	Entrance channel and ATL
ATL porosity	0.7643
Viscous resistance	3.11×10^{10} (1/m2)
Relative viscosity	Breugem
Porous jump thickness	0 (m)
Two sided jump adhesion	enabled
Wall contact angle	130 (deg)
Porous jump contact angle	170 (deg)
Gas inlet velocity	6.38×10^{-4} (m/s)
Liquid inlet velocity	0.968 (m/s)
Outlet boundary	Pressure-outlet

Table 4: Model parameters

Parameter	Method
Multiphase model	VOF
Formulation	Implicit
Volume fraction cutoff	1e-6
Body force formulation	Enabled
Interface modelling type	Sharp
Number of phases	2
Turbulence model	$k-\omega$ SST
Surface tension model	Continuum surface force
Wall adhesion	Enabled
Jump adhesion	Enabled

Table 5: Used solution methods

Equation	Method
Pressure-velocity coupling sch.	SIMPLE
Gradient Spatial Discretization	Least Squares Cell
Pressure Sp. Disc.	PRESTO
Momentum Sp. Disc.	Second Order Upwind
Volume fraction Sp. Disc.	Compressive
Intermittency Sp. Disc.	First Order Upwind
Turbulent kinetic energy Sp. Disc.	First Order Upwind
Specific dissipation rate Sp. Disc.	First Order Upwind

2.6. Numerical model

Two-phase flow in the PEMEC ATL and micro-channels were modelled in three-dimensional and transient mode. The numerical schemes used in this study are mentioned in Tab. 4 and Tab. 5.

The time-step is limited by Courant number, which is the time taken to empty a cell. The volume of each cell was divided by the sum of the outgoing fluxes in the field adjacent the fluid interface to calculate the number [23].

$$Co = \frac{\Delta t}{\Delta x / U_f} \tag{16}$$

where Δx is the grid size and U_L is the fluid real velocity. A variable time-step is used, which satisfies the maximum Courant number of 0.5 at each time-step. The experiment with similar geometry was carried out in the previous study [**?**]. Here, it was seen that the bubbles / Taylor bubbles move upward with very high speed and an exposure time of 10 (µs) was needed to be able to freeze the bubbles / Taylor bubbles. So, we can conclude that the need for a highly small time-step size is essential and physical. The time-step size in ANSYS Fluent is set to vary between 1×10^{-16} to 1×10^{-3}.

3. Results and discussion

3.1. Grid

Figure. 5 and Fig. 6 show the structure of the generated mesh. Three different cell types are shown in the

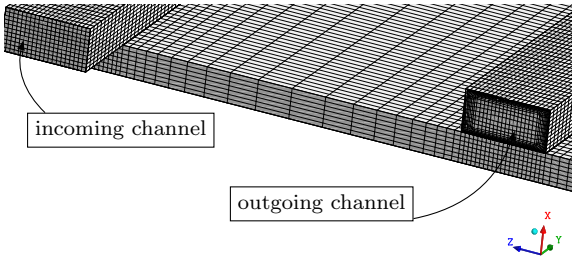

Figure 5: Three dimensional geometry of the incoming / outgoing channels and the ATL with structured mesh types.

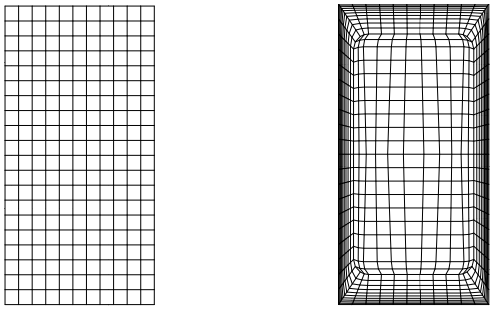

(a) incoming channel (b) outgoing channel

Figure 6: Mesh types of the incoming and outgoing channels. (a) square cells in the incoming channel. (b) square cells at the centre and narrow cells at the areas close to the wall of the outgoing channel.

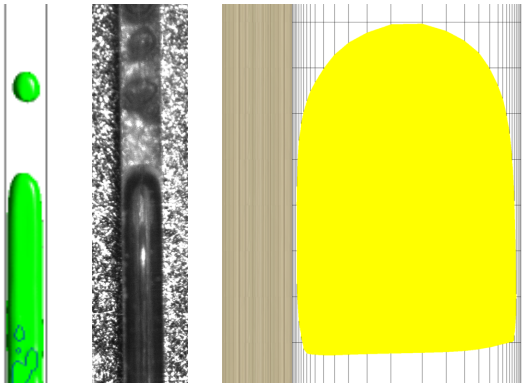

(a) (b) (c)

Figure 7: Comparison of a) the simulation result with b) the experimental photo, c) a Taylor bubble in the meshed channel.

figure for the incoming channel, the ATL and the outgoing channel. It is assumed that only water (i.e. no gas) flows in the incoming channel. The low velocity results in a low Reynolds number of 864, which means that flow is laminar. Only square cells are therefore used for the incoming channel cross sectional area.

In most of the gas—liquid flow within the micro-channels, there is a narrow film layer of water. Highly narrow cells are used close to the walls to capture the water wall film layer that exists especially around Taylor bubbles. Cubic cells are used for central areas of the channel to capture the front and rear circular curvature of the Taylor bubbles. Gupta et al. [23] proposed the following equation to calculate wall film thickness, which is a function of capillary number and the channel hydraulic radius:

$$\frac{\delta}{R} = 1.34 Ca^{\frac{2}{3}} \tag{17}$$

where the Capillary number Ca is defined via:

$$Ca = \frac{\mu_L (U_{LS} + U_{GS})}{\sigma} \tag{18}$$

where U_{LS} is liquid superficial velocity and U_{GS} is gas superficial velocity. Gupta recommended considering 5 cells in the film zone. Table. 2 shows calculated wall film thickness at the middle of the four quarters along the outgoing channel length by the above mentioned equations.

In this study, there are 4 cells in the water film area at the bottom of the outgoing channel and more than 5 cells at the top of the channel.

3.2. Validation

Figure. 7 shows a comparison between the shape of the simulated gas—liquid flow and photos taken with a high speed. The front curved shape of the long Taylor bubble and the narrow wall film around it is very close to the experimental photo. The green area in the simulated photo shows the area where the Taylor bubble has zero wall film thickness. The small bubble in front of the Taylor is also very similar in shape and size. The small bubble seen in the experiment has a slightly smaller diameter than the channel width.

The material properties of the wall are specified to be those of Plexiglas, since the experimental transparent flow plate is made of Plexiglas. This means that the gas—liquid wall contact angle is set to 130 degrees. By default, there is no option to specify the wall contact angle at the porous media-channel interface. This means that the effect of the bubble flowing out of the ATL to the micro-channel cannot be captured, instead the bubbles will stick to the ATL. However, in reality the porous media is hydrophilic and has a contact angle of 170 degrees. To include this effect in ANSYS Fluent, a porous jump is defined at the ATL-channel interface with zero pressure resistance and a gas—liquid contact angle of 170 degrees.

Figure 7 (c) shows a small Taylor bubble in the micro-channel, with a shallow layer of liquid on both the right (i.e. on wall) and the left (i.e. ATL) sides of it.

3.3. Bubbles flow

Figure. 8 shows the bubble shape along the length of the outgoing channel at a specific time step. The figure is separated in three: bottom (a), middle (b) and the top (c) section of the channel. The plot shows Taylor bubbles along the whole length of the channel with some small bubbles between the long Taylor bubbles. At the bottom of the channel, bubbles stick to the wall. Towards the middle of the channel length, a shallow layer of water film forms.

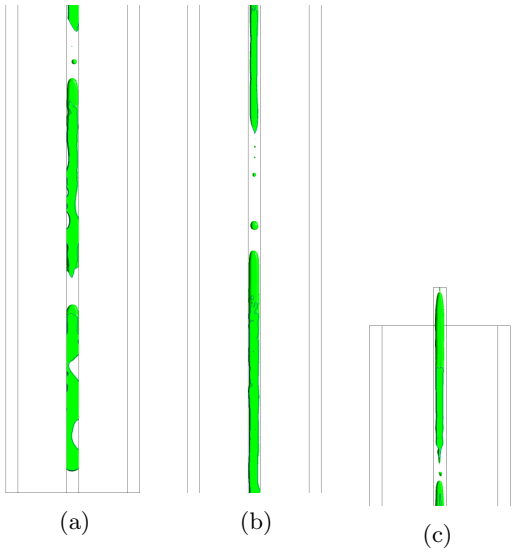

Figure 8: Taylor bubble along the length of the outgoing channel with some small bubbles in between (at a specific time step), a) bottom, b) middle and c) top of the channel.

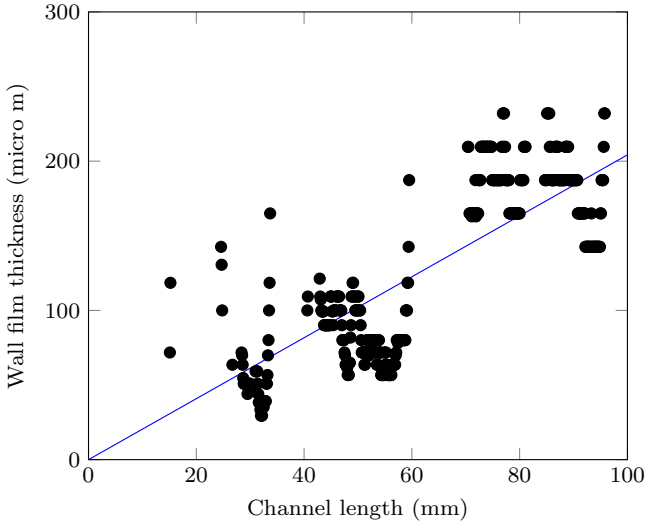

Figure 9: Water film thickness on the micro-channel wall, from bottom to the top of the outgoing channel.

The thickness increases as the bubbles move to the top of the channel. The second bubble in the Fig. 8(a) seems to have a shallow layer of wall film. The wall film on the third bubble of the figure (b) is visible and as the bubble flows up, the film thickness gets thicker. Small bubbles are getting continuously added to the channel from the back permeable wall, and makes the Taylor bubbles larger as they move upward. Water also flows continuously to the channel from the rear permeable wall.

Figure. 9 shows a graph of the measured wall film thickness of the simulation at the outgoing channel. At the bottom of the channel, the wall has a zero liquid film thickness, which means the long Taylor bubbles stick to the wall. This reduces the speed of Taylor bubbles that move upward significantly and essentially creates accumulation effect. This accumulation then makes Taylor bubbles longer with time. Fig. 8 (a) shows that due to the blockage of the channel by the Taylor bubbles, it is seen that the liquid pushes itself into the long bubbles to separate them into two or three Taylor bubbles. The second quarter of the channel has a wall film thickness of about 50 (µm). The third quarter thickness is in between 50 to 100 (µm) and the last quarter is in between 150 to more than 200 (µm).

Figure. 10 shows photos taken from the central section of a test bench that is made similar to the simulation and are taken with the speed of 30 frames per second (fps). Images (a) to (f) shows a long Taylor bubble surrounded by smaller bubbles moving upward.

Figure. 11 shows iso-surface of gas volume fraction of 0.5 by time (a to d). The equivalent speed of images of the simulation is also close to the test photography speed (30 fps). The green colour of the bubbles shows the areas which have zero wall thickness. The test bench reveals

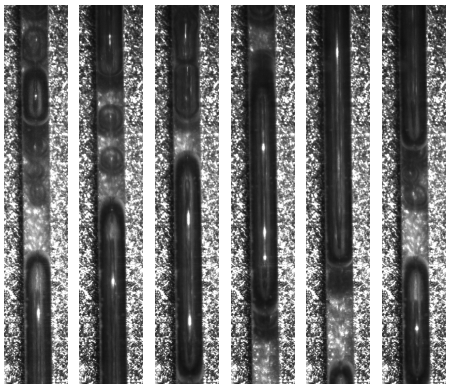

Figure 10: Photos of small bubbles and long Taylor bubbles moving upward in a transparent micro-channel, with the time period of $\frac{1}{30}$ second from (a) to (f).

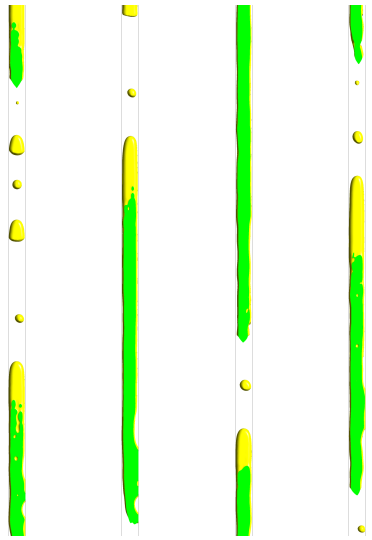

Figure 11: Iso-surface of gas volume fraction of 0.5 in the outgoing channel shown with the time period of 1/30 second from (a) to (d).

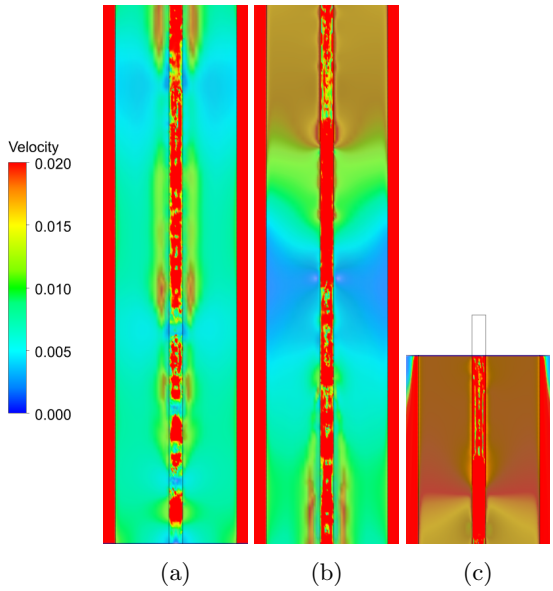

Figure 12: Contour of velocity magnitude on the ATL mid-plane. The legend is limited to 20 mm/s.

the same pattern as seen in the simulation. Especially the shape of the head of the Taylor bubbles are very similar.

3.4. Bubble accumulation

Figure. 12 shows a volumetric render of the velocity magnitude field in the ATL at a specific time. The contour scale is limited between 0 and 20 (mm/s). When examining the velocity distribution, it becomes apparent that it is highly uneven along the length of the channels. Although the velocity distribution within the first half (i.e. Fig. 12 b) only depicts minor local variations, particularly near the outgoing channel, very large changes are seen towards the end of the second half (i.e. Fig. 12 b and c). Moreover, along the length of the second half, zones of both very low and very high velocities are seen. In the following, it will be shown that these differences appear due to a combination of gas accumulation within the ATL and the presence of long Taylor bubbles blocking the entrance to the outgoing channel.

The extent and locations of gas accumulation can be seen by studying Fig. 13. In this figure, the position of the gas—liquid interface in the through-plane direction is shown. A distance of zero equals the position of the interface between the ATL and the catalyst layer, while a distance of 0.35 mm equals the interface between the ATL and the bipolar plate. The plot shows that the gas phase tends to move along the catalyst layer and towards the outgoing channel. When the gas phase moves within a certain distance of the outgoing, the gas phase begins to spread in the through-plane direction towards the outgoing channel. Meanwhile, it appears that this trend depends on the position along the length of the channels. In the first half, the gas phase appears to spread out more and ends up covering a larger volume of the ATL. In the second half, this phenomenon is much less pronounced. A comparison between Fig. 12 and 13 shows that the difference in accumulation of the gas phase from bottom to top coincide well with the observed velocity distribution. Hence, supporting the claim that gas accumulation is the cause.

Further examination of the gas volume fraction distribution and the velocity streamlines depicted in Fig. 14, substantiate these conclusions even further. From the horizontal planes along the length of the geometry, it is clearly seen that the gas phase tends to accumulate near the outgoing channel, particularly in the beginning of the channel. According to the number of streamlines, which correspond to flow rate, a high mass flow rate of water is seen at the second half of the geometry. This very well illustrates that the liquid phase tends to move around the less gas accumulated areas, pressure loss along this path is much lower.

It should be noted here that the Ti-felt is highly hydrophilic. This means that the capillary pressure has a high impact on the uniformity of the water distribution. In this study, the capillary pressure effect is not considered, since a single equation VOF model is used. Improved predictability could however be obtained by developing a multi-fluid VOF model that both accounts for capillary pressure in the porous region and surface tension forces in the channel. The impact of such a model would be to even out the gas distribution.

Figure. 15 shows a cross sectional view of the gas volume fraction at different locations of the channel. It can be seen that bubbles stick to at least one of the walls in all the cross sections. It appears that this phenomenon is due to the rectangular shape of the channel. As mentioned before, a zero wall liquid film reduces the velocity of the upward moving bubbles. As opposed to a rectangular channel, a square channel can probably reduce this effect,

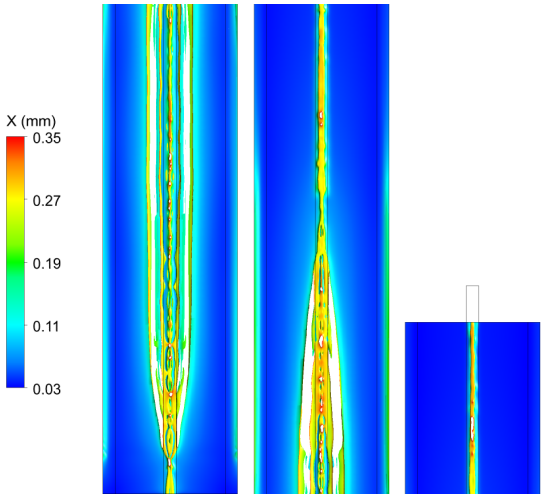

Figure 13: Iso-surface of gas volume fraction of 0.5 in the ATL coloured by its position from the catalyst layer (0 on the ATL-catalyst layer interface and 0.35 mm on the ATL-flow plate interface).

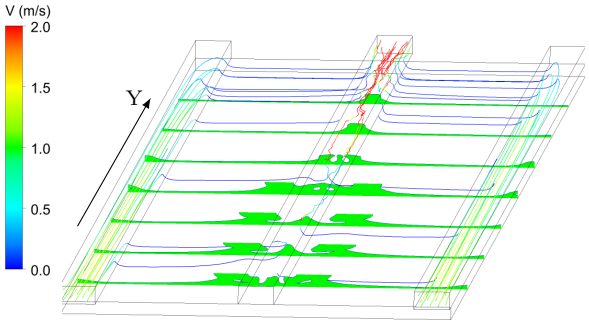

Figure 14: Horizontal plates along the gas phase coloured by gas volume fraction with streamlines from the entrance channel to the outlet.

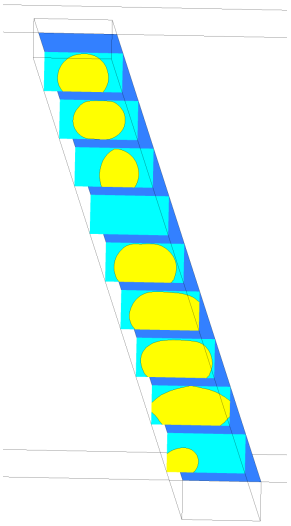

Figure 15: Cross sectional view of the gas volume fraction at different locations of the outgoing channel shows the bubbles sticking to the wall.

since it will allow bubbles to become circular in shape with thin film layer around it. This will then most likely reduce the bubbles tendency to stick to the wall and lower gas accumulation. Another impact can then be that a shift in the transition from bubbly flow to Taylor flow occurs. This can then cause so more bubbly flow is observed in the channel.

To illustrate how the two-phase flow in the microchannel affects the distribution of liquid phase in the incoming channel, the contour plot of the velocity magnitude can be shown together with a volumetric render of the gas volume fraction. By furthermore doing so at two different times, where a shift from bubbly flow to Taylor flow has occurred, the impact of two-phase flow in the microchannel is clearly illustrated. In Fig. 16a, the impact of bubble flow can be observed. In the top section of the incoming channel, a high velocity area is seen. When comparing this velocity increase and its location along the length of the channel to the same location in the outgoing channel, it appear that the behaviour is triggered by the presence of small bubbles. In Fig. 16 b, the impact of Taylor bubbles is conversely shown. At the same location as previously discussed, a nearly uniform velocity distribution is seen. When again comparing the two same locations in the in- and outgoing channels, it becomes clear that a long Taylor bubble in the outgoing channel causes this behaviour. From Fig. 16 a and b, it can furthermore be concluded that a non-uniform distribution of gas along the outgoing channel length creates a non-uniform pressure resistance along the inlet channel. This difference in the flow resistance results in variation in water flow from the inlet channel to the ATL, which correspondingly results in a maldistribution of water in the Ti-felt. Hence, it can be

hypothesised that a more uniform gas—liquid flow regime such as bubbly flow or annular flow will result in a uniform distribution of water in the ATL.

4. Conclusion

gas—liquid flow through an inter-digitated flow field of PEMEC has been analysed numerically with a three-dimensional, transient VOF model in ANSYS Fluent 17.2. To reduce the complexity of the modelled phenomena, the effect of electro-chemistry was neglected, and only the anode side channels and ATL was considered. A fixed source of the gas (air) was implemented at the ATL-catalyst layer interface that corresponds to oxygen evolution reaction. The gas—liquid flow was analysed numerically in the porous medium and the channel. A coarse mesh at the centre of the outgoing channel and a fine mesh close to the wall was used to capture the narrow wall water film along the micro-channel wall. Wall gas—liquid contact angle on the channel wall surface and the ATL-channel interface was considered. The numerical simulation was validated with the pictures taken from the bubbles in micro-channel. These pictures were obtained with an experimental setup that was made for a qualitative comparison of the formed bubbles in the micro-channels. Long Taylor bubbles with small bubbles in between was seen in both the simulation and the experiment. It was seen in the simulation that the wall film thickness changes due to the difference in phase superficial velocities from bottom to the top of the outgoing channel. Results showed that the wall water film thickness increases from 0 at the bottom to 200 µm at the top of the outgoing channel. In reality, there should be a film of water that surrounds all the Taylor bubbles from bottom to the top of the channel, however this was not seen specially at the bottom of the outgoing channel in this simulation. A wall boundary layer mesh that gradually increases from bottom to the top of the channel and adapts itself with the simulated film thickness could potentially solve this issue and hence avoid that gas sticks to the wall. It was also observed that the non-square shape of the channel affects how the Taylor bubbles stick to the wall. The direction where the distance to the opposing wall is shortest, the Taylor bubbles appear to stick to the wall. This effect needs more analysis in a more detailed CFD model.

Furthermore, the results showed that the distance between the Taylor bubbles effect the uniformity of the liquid flow within the incoming channel. A long Taylor bubble, or what essentially amounts to an annular flow, could appear to make the flow of liquid within the incoming channel and the porous media more uniform. A more detailed model that accounts for capillary forces within the porous structure could potentially reveal this with more certaincy. At this point, there is no simple method for predicting behaviour of the flow within the micro-channels, however a detailed CFD model can give in-depth information about the fluid dynamical interactions within a PEMEC. With this knowledge an optimised design could potentially be obtained.

This numerical model is an starting point in the development of detailed PEMEC model that can capture all the essential phenomena governing performance. For future work, it will be attempted to develop a multi-fluid VOF model that includes the porous media capillary pressure effect. The model will similarly include all of the parameters so far considered, i.e. wall contact angle on the porous media within the micro-channel. Another key issue to investigate, is the impact of the gas phase accumulating in the incoming channels and how it affects the distribution of liquid water and bubbles in the outlet channel.

Acknowledgement

We acknowledge the funding provided by Innovation Fund Denmark.

Nomenclature

α	Volume fraction, -
δ	Wall film thickness, m
ϵ	Porosity, -
κ	Kinetic energy, $m2/s^2$
μ	Viscosity, kg/s.m
ω	Turbulent eddy frequency, 1/s
ρ	Density, kg/m^3
σ	Surface tension, N/m
$\mathbf{n}$	Unit normal vector, -
$\mathbf{V}$	Velocity vector, m/s
Ca	Capillary number, -
Co	Courant number, -
CP	Compression pressure, Pa
F	Force, N
g	Gravity, $kg/m^2.s^2$
K	Permeability, m^2
M	Momentum source, m/s^2
p	Pressure, Pa
R	Channel hydraulic diameter, m
Re	Reynolds number, -
s	Strain, -

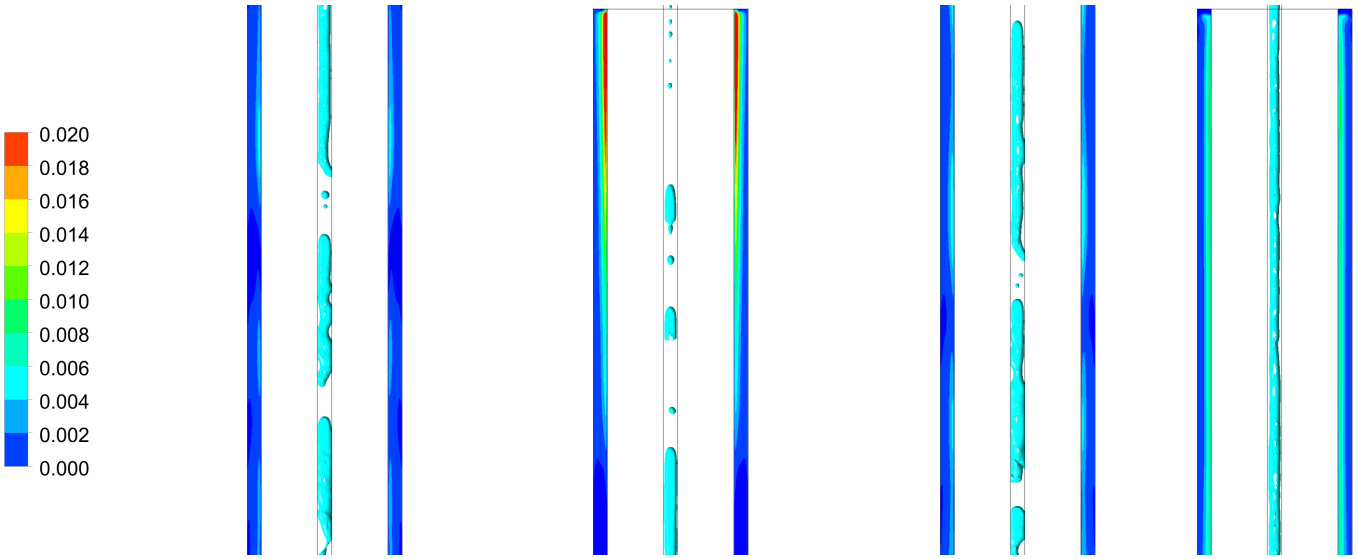

Figure 16: Contour of velocity at the channel-ATL interface in the incoming channel and iso-surface of gas volume fraction of 0.5 in the outgoing channel. They are shown for two different time steps. a) first half b) second half, c) first half, d) second half of the geometry.

t	Time, s
u	Velocity magnitude, m/s
We	Weber number, -

Abbreviations

ATL	Anode transport layer
CCM	Catalyst coated membrane
CFD	Computational fluid dynamics
MEA	Membrane electrode assembly
PEM	Proton exchange membrane
PEMEC	Proton exchange membrane electrolysis cell
Ti	Titanium
VOF	Volume of fluid

Subscripts

α	Phase
0	Initial
e	Effective
f	fluid
G	Gas phase
g	Gas phase
L	Liquid phase
l	Liquid phase
r	Relative
S	Superficial
s	Surface tension

Highlights

- A two-phase numerical method for detailed CFD modelling of gas—liquid flow in micro-channels and transport layer was presented.
- Both wall gas—liquid and porous media contact angles were included in the simulation to correctly simulate bubble wall detachment.
- A layer of fine cells used in the micro-channel close to walls to capture water wall film.
- Wall water film thickness changes from bottom to the top of the micro-channel.
- Long Taylor bubbles with small bubbles in between was seen in both simulation and experiment.